

# Nonequilibrium effects in ballistic point contacts $Ta - Cu$ and $2H - NbSe_2 - Cu$ . Two-gap superconductivity in $2H - NbSe_2$

N.L. Bobrov<sup>1</sup>

<sup>1</sup>*B.I. Verkin Institute for Low Temperature Physics and Engineering of the National Academy of Sciences of Ukraine  
47 Nauka ave., 61103 Kharkov, Ukraine\**

The  $Ta - Cu$  and  $NbSe_2 - Cu$  heterocontacts have been studied. For  $Ta - Cu$  contacts the theoretical estimation of the value of  $\delta$ -functional barrier at the boundary arising due to the mismatch of Fermi parameters of the contacting metals was carried out and a good agreement between the calculation and experiment was obtained. An expression for the estimation of the diameter of the heterocontact on either side of the boundary is obtained. The magnitude of the jump-like decrease in the excess current (and the superconducting gap) due to the phase transition of the superconductor region near the point contact into a spatially inhomogeneous state when the critical concentration of nonequilibrium quasiparticles is reached has been determined. Obtained dependence of the additive differential resistance on the offsets at the contact arising after the phase transition, due to the excess charge of quasiparticles and the associated reverse current (or additive voltage). In  $2H - NbSe_2$  there is a two-zone superconductivity character with  $\sim 8$  times different energy gap values. Under the influence of current injection of nonequilibrium quasiparticles there is a sequential phase transition of the layers adjacent to the point contact into a spatially inhomogeneous state with a suppressed gap, which is accompanied by a step change in the slope of the  $I - V$  curve with a discrete increase in the differential resistance.

**Keywords:** Yanson point contact spectroscopy, electron-phonon interaction, nonequilibrium superconductivity, energy gap, excess current.

PACS numbers: 71.38.-k, 73.40.Jn, 74.25.Kc, 74.45.+c, 74.50.+r

## CONTENTS

1. Introduction	1
2. Theory	2
3. Experimental Procedure	5
4. Experimental Results	6
4.1. Superconducting gap and nonequilibrium feature in $Ta - Cu$ point contacts	6
4.2. Superconducting gap and nonequilibrium feature in $2H - NbSe_2 - Cu$ point contacts	10
5. Discussion	14
6. Conclusion	15
References	15

## 1. INTRODUCTION

The emergence of spatially inhomogeneous states in three-dimensional superconducting ballistic point contacts is one of the most interesting and understudied in the field of nonequilibrium superconductivity. To date, two papers [1, 2] have been published on this topic. They present the results of studies of the evolution of nonequilibrium features in the spectra of tantalum-based contacts - temperature and magnetofield dependences, as well as dependences on resistance. The position of these features on the  $eV$  axis is determined by the critical power of injection of nonequilibrium quasiparticles. When this power is reached, the superconducting gap in the vicinity of the contact decreases in a stepwise manner. The estimates of the critical concentration of nonequilibrium quasiparticles are close to those at which there is a stepwise transition to a spatially inhomogeneous state and at tunnel injection [3]. In the present publication the main conclusions from [1, 2] are summarized concerning the reasons for the appearance of nonparametric features in the spectra of point contacts.

\* bobrov@ilt.kharkov.ua

$I - V$  curves of  $S - c - N$  point contact is significantly nonlinear. In addition to nonlinearity at bias  $eV \sim \Delta$ , caused by the energy gap, in some cases there can be comparable in intensity nonlinearity of non-spectral nature, caused by nonequilibrium processes in the near-contact region.

In  $S - c - N$  point contacts in many cases there is no local equilibrium between electrons and phonons in the current concentration region. In the superconducting bank there is also no equilibrium between quasiparticle excitations and condensate, which appears in the unbalanced occupancy of the electron- and hole-like branches of the quasiparticle excitation spectrum. Quasiparticles with maximum energy equal to the applied voltage relax, emitting phonons and accumulate in a layer of the order of  $\Delta$  above the ceiling of the energy gap. When their concentration reaches a critical value, a phase transition to a spatially inhomogeneous state with a suppressed gap occurs in the superconductor region adjacent to the point contact. Experiment shows that the phase transition to the suppressed gap state is observed only for an unperturbed superconductor with a perfect lattice. The minimum superconductor volume that can undergo the phase transition cannot be less than the coherence length. Therefore, for superconductors with large coherence length in the region of phonon energies the critical concentration is not reached and non-equilibrium features in the spectra are absent.

## 2. THEORY

Since superconductor-normal metal point contacts (hereafter  $S - c - N$ , here  $c$  is a constriction) are always heterocontacts, we first consider the general trends inherent in them in the normal state and then proceed to how they will exhibit themselves in the transition to the superconducting state. We will consider only ballistic point contacts, which do not have any additional scatterers in the form of impurities, defects, etc. at the boundary. Most of the formulas given below are taken from an earlier publication [4], devoted to finding the point-contact EPI function in tantalum, including when using heterocontacts.

As shown in [5], in direct contact between metals, a  $\delta$ -functional barrier arises at the boundary due to a mismatch in the Fermi parameters of the contacting metals. The resistance of the heterocontact in the presence of a  $\delta$ -functional barrier at the boundary is equal:

$$R_{het}^{-1} = \frac{e^2 S S_F}{(2\pi\hbar)^3} \langle \alpha D(\alpha) \rangle_{v_z > 0}^{1,2}. \quad (1)$$

Here  $\langle \dots \rangle_{v_z > 0}$  denotes averaging over the Fermi surfaces of metals 1 and 2, respectively, under the condition  $v_z > 0$ ;  $S$  is the area of the contact;  $S_F$  is the area of the Fermi surface;  $\alpha = v_z/v_F = \cos \theta$ ; and,  $D$  is the transmission coefficient of the boundary. The quantity  $R_{het}^{-1}$  is independent of the metal over which the averaging is performed, and it is independent of the electron dispersion law, i.e.,

$$\{S_F \langle \alpha D(\alpha) \rangle\}_1 = \{S_F \langle \alpha D(\alpha) \rangle\}_2. \quad (2)$$

Taking into account the fact that

$$\frac{(2\pi\hbar)^3}{e^2 S S_F \langle \alpha \rangle_{v_z > 0}} = \frac{16\pi\hbar}{e^2 k_F^2 d^2} = R_0, \quad (3)$$

where  $R_0$  is the resistance of the homocontact, we obtain  $R_{het} = R_0 (\langle \alpha \rangle_{v_z > 0} / \langle \alpha D(\alpha) \rangle_{v_z > 0})$ . In a metal with a large value of  $p_F$ , the relative phase volume of nonequilibrium filled states is smaller due to the reflection of part of the electron trajectories from the heterogeneous interface. The coefficient of electron passage through the heterogeneous interface is:

$$D = \frac{4v_{z1}v_{z2}}{(v_{z1} + v_{z2})^2}, \quad (4)$$

where  $v_{z1} = v_{F1} \cos \theta_1$ ;  $v_{z2} = v_{F2} \cos \theta_2$ ; If the angle of incidence of the electron on the heterogeneous interface deviates from the vertical, at its intersection the trajectory of the electron experiences refraction. This is due to the fact that when an electron passes from one metal to another, the law of conservation of the tangential component of its momentum must be followed:  $p_{\parallel} = p_{F1} \sin \theta_1 = p_{F2} \sin \theta_2$ . Denote  $p_{F1}/p_{F2} = b$ ;  $v_{F1}/v_{F2} = c$ ;  $\cos \theta_1 = \alpha_1$ ;  $\cos \theta_2 = \alpha_2$ . We assume for definiteness that  $b < 1$ . As a result we obtain

$$\alpha_1 = b^{-1}(\alpha_2^2 + b^2 - 1)^{1/2}; \quad \alpha_2 = b(\alpha_1^2 + b^{-2} - 1)^{1/2}. \quad (5)$$

The transmission coefficients at each bank can be written in the form:

$$D(\alpha_1) = \frac{4b\alpha_1(\alpha_1^2 + b^{-2} - 1)^{1/2}}{c[\alpha_1 + (b/c)(\alpha_1^2 + b^{-2} - 1)^{1/2}]^2}; \quad (6)$$

$$D(\alpha_2) = \frac{4c\alpha_1(\alpha_2^2 + b^2 - 1)^{1/2}}{b\left[\alpha_2 + (c/b)(\alpha_2^2 + b^2 - 1)^{1/2}\right]^2}. \quad (7)$$

For a spherical Fermi surface

$$\begin{aligned} \langle \alpha \rangle_{v_z > 0} &= 1/2; \quad \langle \alpha D(\alpha) \rangle_{v_z > 0} = \int_0^1 \alpha D(\alpha) d\alpha; \\ R_{het}^{-1} &= 2R_0^{-1} \int_0^1 \alpha D(\alpha) d\alpha. \end{aligned} \quad (8)$$

Since  $R_{het}^{-1}$  does not depend on the number of the metal for which the averaging is carried out, we have

$$\begin{aligned} 2\langle \alpha_2 D(\alpha_2) \rangle_{v_z > 0} &= 2 \int_{\sqrt{1-b^2}}^1 \alpha_2 D(\alpha_2) d\alpha_2 \equiv \\ &\equiv 2b^2 \langle \alpha_1 D(\alpha_1) \rangle_{v_z > 0} \end{aligned} \quad (9)$$

The integration for the second metal is performed from  $\sqrt{1-b^2}$ , because of the fact that for  $\alpha_2 < \sqrt{1-b^2}$  the quantity  $D(\alpha_2) = 0$ , since total internal reflection of the electrons from the hetero boundary occurs. The diameter of the heterocontact in this case equals:

$$\begin{aligned} d_{het} &= d_1 [2\langle \alpha_1 D(\alpha_1) \rangle_{v_z > 0}]^{-1/2} = \\ &= d_2 b^{-1} [2\langle \alpha_1 D(\alpha_1) \rangle_{v_z > 0}]^{-1/2} \end{aligned} \quad (10)$$

Here  $d_1$  is the diameter of the homocontact of a metal with a smaller value of the Fermi momentum, and  $d_2$  is the diameter of the homocontact of a metal with a larger value of the Fermi momentum.

From here, knowing the diameter of the homocontact, we can calculate the diameter of the heterocontact, and the result of the calculation does not depend on which side of the metal was calculated.

*Hence, if we consider two different ballistic heterocontacts in which one of the banks is the same metal, their diameters will also be close to each other if the resistance values and the values of the barrier at the hetero boundary are close.*

Let us consider for clarity the heterocontact  $Ta - Cu$ . The diameter of the homocontact can be determined by Sharvin's formula  $d = (16\rho l / 3\pi R_0)^{1/2}$ . In the free-electron approximation:

$$\rho l = p_F / ne^2 = \frac{3\pi^2 \hbar}{k_F^2 e^2} = \frac{1.66 \cdot 10^4}{\{k_F (cm^{-1})\}^2} [\Omega \cdot cm^2]; \quad (11)$$

$$d = \frac{4}{ek_F} \left( \frac{\pi \hbar}{R_0} \right)^{1/2} = 44.49 \frac{10^8 (R[\Omega])^{-1/2}}{k_F [cm^{-1}]} [nm].$$

$$k_F = (3\pi^2 z / \Omega)^{1/3}, \quad (13)$$

where  $z$  is the number of conductivity electrons per primitive cell,  $\Omega$  is the volume of the primitive cell. For a VCC lattice,  $\Omega = a^3/2$   $a$  is the lattice constant. Using the free-electron approximation, the true wave functions are approximated by smooth pseudowave functions. The greatest differences are observed in the region of the core of the atom, which in simple metals is small and occupies about 10% of the volume. In transport phenomena, in particular electrical conductivity, the free-electron approximation in such metals as copper, gold and silver "works" very well. In the VA subgroup for  $V$ ,  $Nb$  and  $Ta$  over the filled shell configuration of argon, krypton and xenon, respectively, there are 5 valence electrons per atom. Due to the small number of electrons filling the d-zones, the Fermi level crosses them, so the band structure of these metals near the Fermi surface is very complex. All metals of the subgroup are uncompensated with a total number of carriers of one hole per atom [6]. Therefore, for tantalum we take  $z=1$  in the free-electron approximation. Note that  $z$  is not always an integer. In [6] there are values of  $z$  for a large number of transition metals, which can be used in estimates of this kind. Given that  $a=0.3296$  nm, we find  $k_F^{Ta} = 1.183 \cdot 10^8 cm^{-1}$ . From the de Haase - van Alphen [7] experiments, the ratio of the effective electron mass averaged over the Fermi surface to the free-electron value  $m^*/m_0 = 1.85$  is determined for tantalum; then  $v_F^{Ta} = 0.74 \cdot 10^8 cm/sec$ . For copper respectively:  $v_F^{Cu} = 1.57 \cdot 10^8 cm/sec$ ;  $k_F^{Cu} = 1.36 \cdot 10^8 cm^{-1}$ ; then for copper and tantalum contact diameters we have respectively:  $d_{Ta} = 37.54 \cdot R(\Omega)^{-1/2} [nm]$ ;  $d_{Cu} = 33.5 \cdot R(\Omega)^{-1/2} [nm]$ ; Then, as follows from the equations  $b = p_F^{Ta} / p_F^{Cu} = k_F^{Ta} / k_F^{Cu} = 0.87$ ;  $c = v_F^{Ta} / v_F^{Cu} = 0.544$ ;

$$\begin{aligned} d_{het} &= d_{Ta} [2\langle \alpha_1 D(\alpha_1) \rangle_{v_z > 0}]^{-1/2} = \\ &= d_{Cu} b^{-1} [2\langle \alpha_1 D(\alpha_1) \rangle_{v_z > 0}]^{-1/2} = 70.2 (R[\Omega])^{-1/2} [nm], \end{aligned} \quad (14)$$

The maximum angle of incidence of the electrons at the interface on the copper side is  $\theta_2^{max} = 60.46^\circ$ .

Instead of the free-electron value  $\rho l$  (Eq.11) we can use values obtained from experiments:  $\rho l_{Ta} = 0.59 \cdot 10^{-11} \Omega \cdot cm^2$  [8];  $\rho l_{Cu} = 0.53 \cdot 10^{-11} \Omega \cdot cm^2$  [9]. For the contact diameters of copper and tantalum we have respectively:  $d_{Ta} = 31.65 \cdot R(\Omega)^{-1/2} [nm]$ ;  $d_{Cu} =$

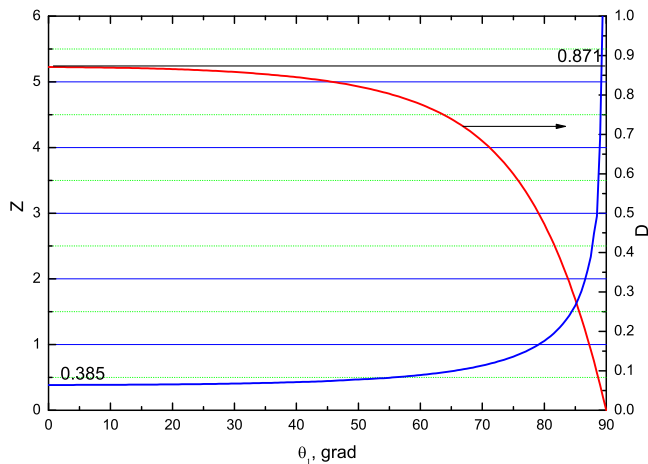


Figure 1. Dependences of the tunneling parameter  $Z$  and the transmittance coefficient  $D$  on the deviation from the normal of the angle of incidence of the electrons on the heterogeneous boundary when calculated from the tantalum shore side in the free-electron approximation.

$30 \cdot R(\Omega)^{-1/2}[nm]$ ; then from the Eq.11 follows:  $b = p_F^{Ta}/p_F^{Cu} = (\rho_{Cu}/\rho_{Ta})^{1/2} = 0.948$ ; Fermi velocity ratio is the same:  $c = v_F^{Ta}/v_F^{Cu} = 0.544$ ; ; then  $d_{het} = 59.2 \cdot R(\Omega)^{-1/2}[nm]$  and the maximum angle of incidence of electrons at the interface on the copper side is  $\theta_2^{max} = 84^\circ$ .

Fig.1 for the  $Ta - Cu$  heterocontact shows the angular dependence of the passage coefficient  $D(\theta_1)$  (Eq.(6), converted into degrees) across the barrier on the heterogeneous interface from the tantalum side in free-electron approximation, and the associated tunneling parameter by the relation:  $Z = \sqrt{(1/D) - 1}$ .

Let us now consider what happens to the heterocontact when one of the banks transitions to the superconducting state. In superconductor-normal-metal (hereafter  $S - c - N$ , here  $c$  stands for constriction) point contacts with direct conduction, the current flowing is determined by a quantum process called Andreev reflection. In this process, the electron moving from the normal metal to the superconductor as it moves away from the heterogeneous interface at the coherence length is converted to a Cooper pair. Toward the electron, a hole from the opposite spin band passes into the normal metal. In the ideal case, in the absence of electron scattering at the boundary, at  $T \rightarrow 0$  for voltages less than  $\Delta/e$  the conductivity of the point contact doubles. An intermediate, between tunneling and barrier-free, mode of current flow in point contacts is described by the Blonder-Tinkham-Klapwijk (BTK) model [10]. The following equation (15) (taken

from [11], equation 5) is a modified version of the BTK equation in the two-gap approximation, which includes the possibility to account for finite carrier lifetime by introducing the  $\Gamma$  broadening parameter. It is used to find the superconducting gaps  $\Delta_1$  and  $\Delta_2$ , the broadening parameters  $\Gamma_1$  and  $\Gamma_2$ , and the tunneling parameter  $Z$ . In the process of fitting, the minimum RMS deviation of points on the theoretical curve from the corresponding points on the experimental curve is achieved. As fitting parameters, in addition to the above, the contribution to the total conductivity  $K_1$  from the gap  $\Delta_1$ , and  $(1 - K_1)$  from the gap  $\Delta_2$  will act as fitting parameters. If the experimental differential resistance curve is normalized to the normal state curve, the scaling factor  $S_F$  can be obtained from Equation 15. This is not a fitting parameter, but an indicator of how much the intensity (or amplitude) of the experimental curve matches the theoretical model. The BTK model and its modifications are one-dimensional, assuming that the charge carriers hit the boundary between the metals along a perpendicular trajectory. Nevertheless, it is perfectly suited, in particular, to find the  $Z$  parameter in  $Ta - Cu$  heterocontacts, given that it follows from Fig.1 that the appreciable growth of  $Z$  (blue curve) begins at angles over  $70^\circ$  from the perpendicular to the contact plane. There is a more complex three-dimensional Zaitsev model in which the transparency coefficient  $D$  can depend on the angle of incidence of the carriers at the interface [12]. A review of [13] in Section 2 also gives the Zaitsev formulas, and Section 7 shows that applying the 3D model gives essentially the same result as the 1D model, except for the slightly different parameter  $Z$  (see Figure 11, [13]).

$$\frac{dV}{dI} = \frac{S_F}{\frac{dI}{dV}(\Delta_1, \Gamma_1, Z)K + \frac{dI}{dV}(\Delta_2, \Gamma_2, Z)(1 - K)} \quad (15)$$

Let us return to the discussion of the parameters in the Eq.(15). The dimensionless parameter  $Z$  characterizes the value of  $\delta$ -functional barrier at the boundary and can vary from 0 to infinity, in fact at  $Z \sim 10$  we have a tunneling contact. The  $\Gamma$  broadening parameter has the same dimensionality as the energy superconducting gap and leads to broadening and suppression of the intensity curves. Let us turn to the  $S_F$  parameter, which is usually left out of the experimental work. In addition to its shape, the theoretical curve normalized to the normal state has a unique amplitude or intensity for each set of the aforementioned parameters. If this amplitude is the same as the experiment, then  $S_F = 1$ . However,

most often it is less than 1, indicating a deviation of the real contact from the theoretical model, for example, not the entire volume is filled with superconductor, or part of the superconductor has reduced superconducting characteristics, etc. As a rule, such deviations are insignificant and can be disregarded. In the single-gap approximation, which is a special case of the two-gap approach, in some cases it is possible to obtain a scaling factor greater than 1. Fig. 18 in [14] shows the dependence of the rms deviation  $F$  of the shape of the theoretical curve from the experimental curve for different values of the superconducting energy gap  $\Delta$  at 7 K. As follows from the figure, there is no pronounced extremum on the curve  $F$  for arbitrary values of  $S_F$ . Nevertheless, such extrema exist for fixed values of the scaling factors, which makes it possible to determine the temperature dependence of the energy gap  $\Delta$  by fixing this parameter. Most often, this happens if the curves are strongly fuzzy (the  $\Gamma$  parameter is comparable or larger than  $\Delta$ ), and the standard deviation of the shape of the experimental and theoretical curves weakly varies over a sufficiently wide range of fitting parameters. In this case, sometimes the minimal standard deviation of the shape of the calculated and theoretical curves corresponds to  $S_F > 1$ . Obviously, in this case one should choose such a set of parameters at which  $S_F < 1$ . A more rare, but more interesting case is when there are 2 closely spaced gaps, which one tries to approximate by single-slit approximation with quite large broadening parameter  $\Gamma$ . If the temperature during measurements is high enough to blur the experimental curve a little, or the gap components are slightly blurred, the shapes of the calculated curves in the one-gap and two-gap approximation will practically coincide, while the scaling factor for the one-gap approximation will be significantly larger. Note that if no phase transitions occur during temperature measurements, the scaling factor remains unchanged. This allows us to reduce the error in calculations of the temperature dependences of the gaps in the region of high temperatures, where the experimental curves are strongly blurred.

### 3. EXPERIMENTAL PROCEDURE

Point contacts were created between the massive electrodes. Single crystals of tantalum, copper, and  $2H - NbSe_2$  were used as electrode materials. The criterion for the quality of the material used in point contact spectroscopy is the ratio of the resistivity at room

temperature to the residual resistance at low temperature  $\rho_{300}/\rho_{res}$ . For a large number of metals and compounds there are known temperature-independent constants  $\rho l$ , where  $l$  is the free path of carriers. Knowing these values, it is easy to estimate the impulse free path length at low temperature, which will be the estimate from above for the elastic electron path length through the point contact. For example, for our tantalum samples  $\rho_{300}/\rho_{res} \sim 20$ ,  $\rho l = 0.59 \cdot 10^{-11} \Omega \cdot cm^2$  [8],  $\rho_{273} = 12.6 \cdot 10^{-6} \Omega \cdot cm$  [15], then the free path in the vicinity of the  $Ta - Cu$  point contact cannot be greater than 90 nm. To create ballistic point contacts it is necessary to use a technology that minimizes the formation of additional scattering centers in the surface layer of the material in the vicinity of the short circuit. As experience shows, it is necessary to completely exclude mechanical processing when making electrodes - cutting, grinding, etc. Copper and tantalum electrodes were cut on an electrical discharge machine in the form of  $10 \div 15$  mm long bars and  $1 \times 1 \times$  or  $1.5 \times 1.5 \times mm^2$  cross sections. For the  $NbSe_2$  experiments, the copper electrodes were cut in the shape of a pyramid with a base of  $1 \times 1 \times$  or  $1.5 \times 1.5 \times mm^2$  and a height of  $4 \div 5$  mm. The defective layer on the electrode surface was removed by chemical or electrochemical treatment in a mixture of concentrated acids. Let us emphasize the importance of this operation - in addition to the removal of the defective layer, the properties of the oxide on the surface are very important. The contact area of the electrodes is many orders of magnitude larger than the point contact area, the supporting oxide ensures its mechanical and electrical stability. The thickness of the oxide should be optimal so that the contact is sufficiently mechanically stable and, at the same time, to minimize the introduction of additional scatterers when creating the short circuit. In addition, its electrical properties are very important - no leakage currents should flow through it, parallel to the current through the point-contact. It is also necessary that there are no intermediate shunt conductive layers between the insulating oxide and the metal. For some metals, this problem has not yet been solved. For copper and tantalum no difficulties have arisen. For the (electro)chemical polishing of tantalum, the mixture consisted of  $HF : HNO_3 : HClO_4$  taken in equal volume ratios, and for copper, from  $HNO_3 : H_3PO_4 : CH_3COOH$  in a 2:1:1 volume ratio. The electrodes were then washed in distilled water, dried, and mounted in a [16] point contact device. Surface quality control after (electro)chemical



treatment was performed using an optical microscope in oblique light. The working surface should be free of dirt and off color. The rounding radius of the pyramidal apex was  $r \leq 0.1mm$ .

The  $3 \times 5 \times mm^2$  electrode was cut with a blade from a  $NbSe_2$  single crystal of about  $\sim 0.1mm$  thickness and bonded with silver paste to a wire holder. Immediately before measurements, the top layers were removed, ensuring that the copper counterelectrode touched the inner, perfect layers. Note that on the natural growth faces of the monocrystal superconductivity is usually partially suppressed.

The device for creating point contacts allowed to smoothly change the pressure force between the electrodes and move them relative to each other [16]. To ensure stability of the contacts, one of the electrodes is attached to a damper.

The  $Ta - Cu$  contacts were created using the shear method [4, 17] in two steps. First, the electrodes were touched by the edges and then shifted relative to each other. The resistance of the resulting contacts was continuously monitored. Contacts with a resistance of several hundred ohms to several kilohms were selected for the next stage. By regulating the strength of the electrodes pressed against each other, such contacts were obtained quite often. Then with the help of the decade resistor connected in series with the voltage source and the found point contact we began to increase the current in steps. Resistance of the point contact also decreased in steps. The breakdown voltage at the contact was  $500 \pm 200$  mV. When the desired resistance interval was reached, the contact was held under the final current for several minutes. Resistances of good quality point contacts obtained by this method ranged from 30-40 to 200-250  $\Omega$ , the quality criterion being the EPI spectra. The highest parameters of spectra showed point contacts with resistance of 50-80  $\Omega$  [4]. The point contacts obtained by this method were of much higher quality than those obtained by the standard shear method and had better mechanical and electrical stability.

The  $Cu - NbSe_2$  point contacts were created using the standard shear method [17] - the top of the copper pyramid was pressed against the  $NbSe_2$  surface with a small force and then shifted parallel. Varying, if necessary, the pressing force, we obtained a point contact for subsequent measurements.

## 4. EXPERIMENTAL RESULTS

### 4.1. Superconducting gap and nonequilibrium feature in $Ta - Cu$ point contacts

For the experimental estimation of the barrier value in the heterocontact due to the mismatch of the Fermi parameters, the point contacts should be ballistic and have no additional scatterers in the contraction plane. The BTK equation [10] and its modification [11] refer to the ballistic mode of electron flight through the point contact. As shown in [18], in the diffusion mode the first derivative of the  $I - V$  curves with parameter  $Z = 0$  practically coincides in form with that in the ballistic mode with tunneling parameter  $Z = 0.55$ . The corresponding illustration can be seen in the overview [13] in Fig. 9. One can distinguish the diffusion contact from the ballistic contact by the appearance of the second derivative of the  $I - V$  curves. The decrease in the elastic electron scattering length is due to an increase in the number of scatterers, i.e., an increase in the concentration of impurities and lattice defects, which leads to distortion of the crystal lattice of the metal. And since nonequilibrium phonons reflect the vibrational structure of the material in the vicinity of its generation, as the elastic relaxation length decreases, there is a broadening of the EPI peaks in the spectra, the suppression of high-energy phonon features up to their complete disappearance and to the growth of the background. In [19] the effect of Nb point contact contamination on the EPI spectra was considered.

A more complicated case is the identification of the scatterers on the heterogeneous boundary. The influence of the translucent boundary wall on the appearance of the second derivative of the  $I - V$  curve (T-model) is considered in [20]. It shows that the intensity of the phonon peaks in the spectra is inversely proportional to the transparency coefficient. At the same time, the intensity of the two-phonon processes decreases much slower. Thus, the relative intensity of the two-phonon processes on the second derivatives in the normal state can be used to judge the presence of such a boundary. Note that the low intensity of the EPI spectra in the absence of their broadening and low background level is not an unambiguous sign of the T-model and may be due to multi-contact (small-diameter contacts included in parallel have a lower spectrum intensity than a single point contact with the same resistance), or a strong deviation of the short circuit shape from the circular hole (for example, a long crack

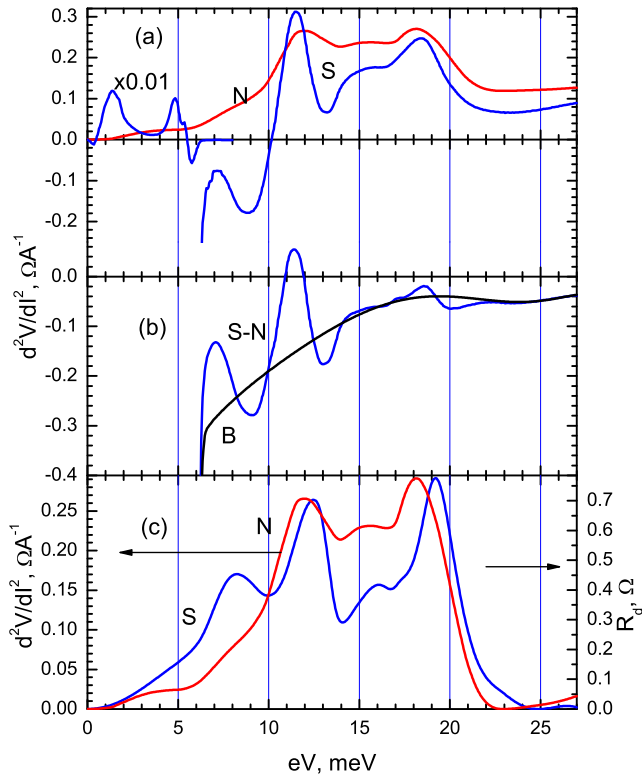


Figure 2. (a) Second derivative of the  $I - V$  curve of the  $Ta - Cu$  point contact in the normal ( $N$ ) and superconducting ( $S$ ) states. The initial area of the  $S$ -spectrum is reduced in intensity by a factor of 100.  $H=0$ ,  $T_N=4.3$  K,  $T_S=1.7$  K,  $R_0^N=73\Omega$ . (b)  $S - N$  is the difference between the second derivatives of the  $I - V$  curve,  $B$  is the background curve. (c)  $N$  is the second derivative of the  $I - V$  curve of  $Ta - Cu$  point contact in the normal state after the background correction;  $S$  is the differential resistance proportional to the EPI function obtained from the superconducting addition to the spectrum after subtracting the background curve ( $S - N - B$ ).

in the backing oxide).

Thus, the simplest test, a kind of passport characterizing the mode of electron passage through the point contact, is the form of the second derivative of the  $I - V$  curve in the normal state. Figure 2(a),(b) shows the second derivatives of the  $I - V$  curves of the  $Ta - Cu$  point contact in the normal and superconducting states, as well as the difference curve and superconducting background curve, and Fig. 2(c) are the curves proportional to the EPI function obtained from these spectra. The procedure for correcting the background and restoring the EPI function from the superconducting additive to the spectrum is described in detail in [19]. The large intensity of high-energy phonon peaks and pronounced van Hove features, unequivocally testify to the ballistic flight

of electrons through the point contact and unperturbed tantalum crystal structure in the volume, on the order of the coherence length, where the formation of phonon nonlinearity in the superconducting state [21] occurs.

Let us now turn to the initial region of the second derivative of the superconducting state point contact  $I - V$  curves (Fig. 2(a)). Along with the nonlinearity due to the  $\Delta$  energy gap in the quasiparticle excitation spectrum, there is a feature on the curve due to a jump change in the superconductor properties in the nonequilibrium state (phase transition) when reaching the critical concentration of nonequilibrium quasiparticles in the near-contact region [1, 2]. For different contacts, the position of such features depends on their resistance, temperature, and/or external magnetic field. During the transition to the superconducting state, the nucleation of such features occurs near the characteristic phonon energies (low-frequency phonon mode, the first or second phonon peak, depending on the contact resistance). As the temperature decreases, their intensity increases, and they shift to lower energies. At a fixed temperature, the position of the features on the energy axis is proportional to  $R^{1/2}$ , which corresponds to the constancy of the critical power  $P_c = V_c^2/R \simeq \text{const}$  ( $\simeq 0.4\mu\text{W}$  at 2 K). The effect of the magnetic field is similar to that of temperature - the feature is blurred, its intensity decreases, and it shifts to the region of higher energies. The corresponding temperature and magnetic-field dependences are shown in Figs. 8-10 in [2]. Since reaching the critical concentration of quasiparticles above the gap depends on the ratio of the rate of their generation, determined by the power, and the recombination (escape) rate, which increases with temperature and magnetic field, this explains the similar temperature and magnetofield dependence of the position of features on the energy axis.

Fig.3 shows the differential contact resistances in the normal and superconducting states (panel (a)), as well as the normalized  $Exp = R_d^S/R_d^N$  curve and the calculated  $Calc$  curve (panel (b)). Panel (c) shows the curves from panel (b) on a larger scale. As follows from the parameters of the calculated  $Calc$  curve shown in the figure, there is a good agreement in the value of the obtained tunneling parameter ( $Z=0.307$ ) with the estimate of the same at the perpendicular electron falling on the interface ( $Z=0.385$ , fig.1). The discrepancy, apparently, is connected with roughness of estimation of the ratio of Fermi speeds of contacting metals. Hence, we can assume that the other estimates (e.g., for the diameter of

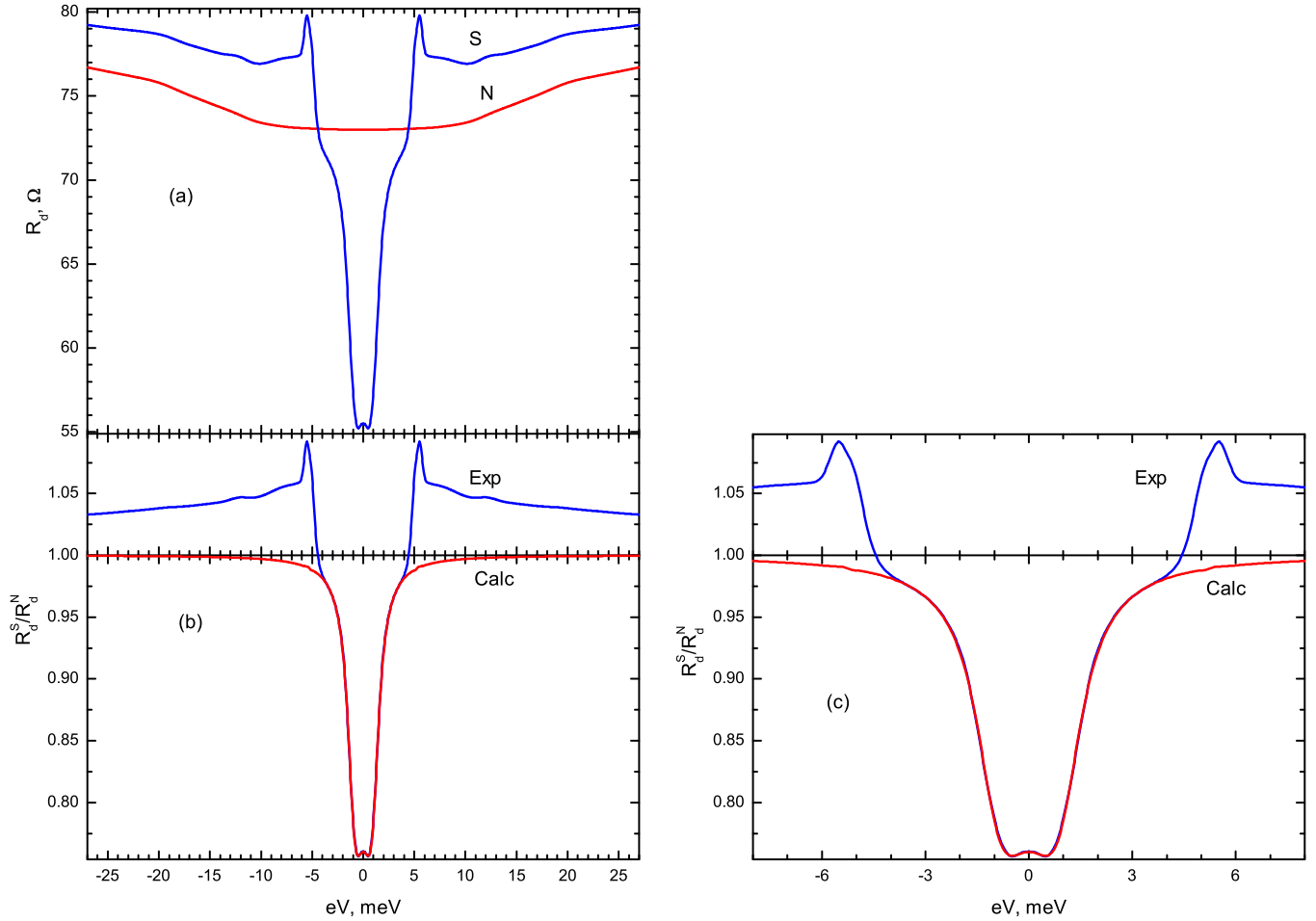


Figure 3. (a) - differential resistances of the  $Ta - Cu$  heterocontact shown in Fig.2, in normal ( $N$ ) and superconducting ( $S$ ) states. (b) - differential resistance after normalization (Exp), and the calculated curve (Calc). (c) - the curves shown in (b) on a larger scale.  $T=1.7$  K,  $\Delta=1.04$  meV,  $Z=0.307$ ,  $\Gamma=0.38$  meV,  $S_F=0.99555$

the heterocontact) are also quite adequate. Also, based on the proximity of  $S_F$  to 1, the superconducting properties of the contact are consistent with the theoretical model.

The shape of the nonequilibrium feature corresponds to a jump-like decrease in the excess current observed as the difference of the  $I - V$  curves in the  $S$  and  $N$  states [22], and is accompanied by an increase in the differential resistance. If to calculate the value of excess current from bias on the contact use experimental curves of differential resistance in the normal  $N$  and superconducting  $S$  states (Fig.3(a)), the excess current becomes negative (Fig.4(a)) at voltage over 16 mV. This does not make physical sense and reflects the fact that the superconducting state  $I - V$  curve has a larger slope and crosses the normal state  $I - V$  curve. In order to correctly estimate the dependence of the excess current on the bias, it is necessary to take into

account the change in this slope in the vicinity of the nonequilibrium singularity. For this purpose, let's find the differential contact resistance dependence on the bias in the superconducting state without taking into account the EPI.

In panel (d) the second derivatives of the  $I - V$  curve are shown, in which there are no spectral components. The *exp* curve in the initial section coincides with the curve  $S$  in Fig. 2(a), and when the voltage exceeds 6 mV it coincides with the background curve  $B$  in Fig.2(b). The *calc* curve is obtained by differentiating the calculated curve in Fig.3(b) and scaled accordingly. Panel (e) shows the differential resistances corresponding to these curves, as well as the differential normal state resistances for the calculated *calc* curve, which is a horizontal line at  $73\Omega$ , and the corrected differential normal state resistivity curve for the experimental *exp* curve. It consists



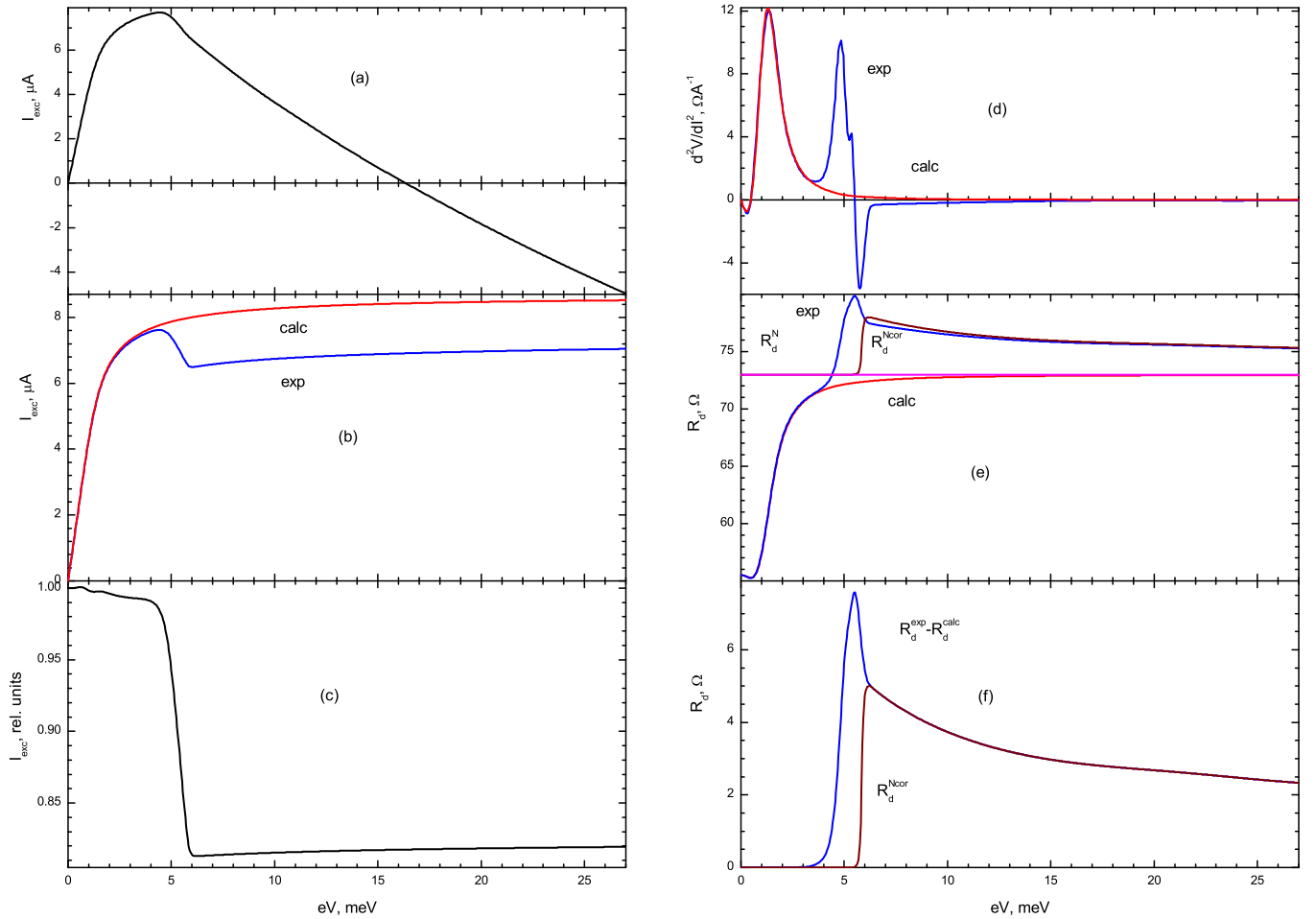


Figure 4. (a) Excess current calculated using experimental differential resistance curves, for superconducting and normal states, shown in Fig.3(a). (b) The same, for the curves shown in (e). (c) The relative value of the excess current from the bias at the contact. (d) are the second derivatives of the  $I - V$  curve obtained after subtracting the nonlinearities due to the EPI. The *exp* curve in the initial section coincides with the curve  $S$  in Fig.2(a), and at  $eV > 6$   $meV$  coincides with the background curve  $B$  in Fig.2(b). The *calc* curve is obtained by differentiating the calculated curve in Fig.3(b) and scaled accordingly. (e) *exp* and *calc* are the differential resistances corresponding to the second derivatives in panel (d),  $R_d^N = 73 \Omega$  is the normal state differential resistance for curve *calc*,  $R_d^{Ncor}$  – corrected normal state differential resistance for curve *exp*, details in text. (f) The difference resistance differential and the corrected normal curve  $R_d^{Ncor}$ .

of three parts. The initial segment coincides with the straight line, the second segment represents the difference between the differential resistances of the experiment and the calculation at a bias greater than 6 mV (panel (f)). The stepped segment conjugates the two parts  $R_d^{Ncor}$ . Such an unusual, at first glance, choice of the shape of this curve is related to the need to eliminate the influence of the differential resistance jump (break in the  $I - V$  curves) when finding excessive current. The differential resistance difference from the contact bias shown in panel (f) shows a maximum around 5.5 mV, a value of 7.58  $\Omega$  or  $\sim 10\%$  of the contact resistance in the normal state at zero bias. This value is an order of magnitude

greater than the spectral component proportional to the EPI function (Fig.2(c), curve  $S$ ).

Fig.4(b) shows the dependences of excess current values on the contact bias *calc* and *exp*, calculated from the differential resistance curves shown in panel (e), and panel (c) shows the relative value of excess current drop when the near-contact region enters the nonequilibrium state. As follows from the figure, the excess current suppression is less than 20%.

Fig. (5) compares the contribution to the differential resistance of a point contact in the superconducting state from nonequilibrium processes and electron-phonon interaction.

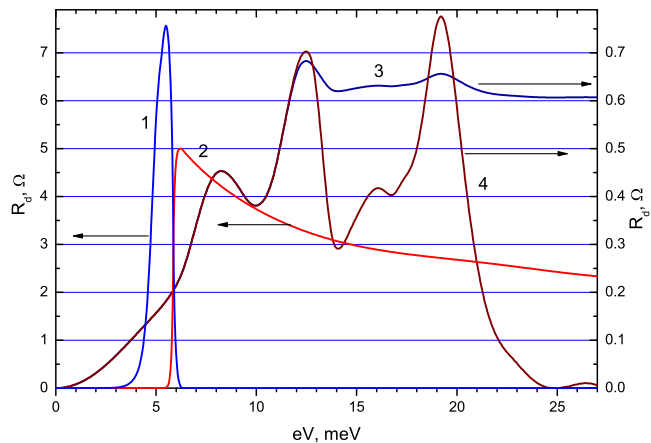


Figure 5. Comparison of the relative magnitude of additional nonlinearities in the superconducting state associated with nonequilibrium processes in point contacts and with EPI: 1 - jump of differential resistance of the point contact, corresponding to the reduction of excess current during the transition of the superconducting region near the contact to the nonequilibrium state; 2 - additional differential resistance arising as a result of imbalance of occupancy of hole and electronic branches of quasiparticle excitation spectrum, appearance of reverse current and related additional voltage; 3 - change of differential resistance of point contact due to scattering of andreef electrons on nonequilibrium phonons; 4 - the same, after background correction.

Qualitative explanation of the increase in the differential resistance of the point contact during the transition to a nonequilibrium state is based on the appearance of reverse current and the associated additional voltage that increases the contact resistance due to the imbalance of the occupancy of hole and electronic branches of the excitation spectrum of quasiparticles [1, 2]. Through the  $N - S$  boundary, quasiparticles with maximum energy  $eV \gg \Delta$  are injected into the superconductor, which populate the electron-like or hole-like branches of the excitation spectrum, depending on the polarity of the applied voltage. The excitations relax relatively quickly, emitting phonons and accumulating in a layer on the order of  $\Delta$  above the ceiling of the energy gap. Further relaxation of the residual population unbalance of excess quasiparticles occurs rather slowly, over a time of the order of  $\tau_0 \sim \tau_{ep}(\Delta)$  [23], during which the excitation manages to diffuse deep into the superconductor to a distance  $\lambda_Q \sim (l_i l_\Delta)^{1/2}$ , where  $l_\Delta = v_F \tau_0$ . Since the potential difference falls at a distance of the order of  $d$  from the contact plane, similar to what happens in tunneling  $S - I - N$  contacts, in the near-contact re-

gion the chemical potential of quasiparticles is not equal to the chemical potential of pairs. Here there is an excess charge of quasiparticles and the associated reverse current (or added voltage), which increases the contact resistance the greater the charge value. Factors that reduce the magnitude of the unbalance (inelastic scattering on phonons, superconducting current, etc.) reduce the reverse current and contact resistance.

The shape of the differential resistance curve at voltages greater than the critical one is determined by the dependence of the relaxation rate on  $eV$ . As the voltage increases, the injection increases, but the relaxation rate also increases at the same time. At not too large offsets, the increase in the relaxation rate outpaces the injection, and therefore  $\Delta$  tends to grow in a certain voltage range, which determines the anomalous curvature of the differential resistance curve. At large displacements, the increase in the relaxation rate slows down and the gap begins to decrease.

For example, increasing the bias on the contact leads to an increase in the frequency of electron-phonon scattering and, consequently, to a decrease in the additional resistance.

#### 4.2. Superconducting gap and nonequilibrium feature in $2H - NbSe_2 - Cu$ point contacts

Part of the results presented in this subsection was previously published in [24], dedicated to the consideration of spatially inhomogeneous discrete states of superconductors. Here this material is significantly expanded, the emphasis is placed on the importance of taking into account the non-equilibrium processes in the observed effects.

$NbSe_2$  is a layered easily split superconductor with a very high degree of anisotropy. It is formed by three-layer "sandwiches": selenium layer - niobium layer - selenium layer. In each layer, atoms form a tightly packed triangular lattice. The lattice parameters  $a \approx 0.345$  nm;  $c \approx 1.254$  nm; the lattice period along the  $c$  axis contains two monolayers [25]. The strong anisotropy here is due to the weak van der Waals interaction between the selenium layers closest to each other, located in different structural sandwiches. In the normal state at room temperature  $\rho_{\parallel} \sim 2 \cdot 10^{-4} \Omega \cdot \text{cm}$ ;  $\rho_{\perp} \sim 10^{-3} \Omega \cdot \text{cm}$  [26], which is two orders of magnitude greater than the resistivity of typical metals. The coherence length for the unperturbed material is:  $\xi(0)_{\parallel} \approx 7.8$  nm,  $\xi(0)_{\perp} \approx 2.6$  nm, i.e., perpendicular

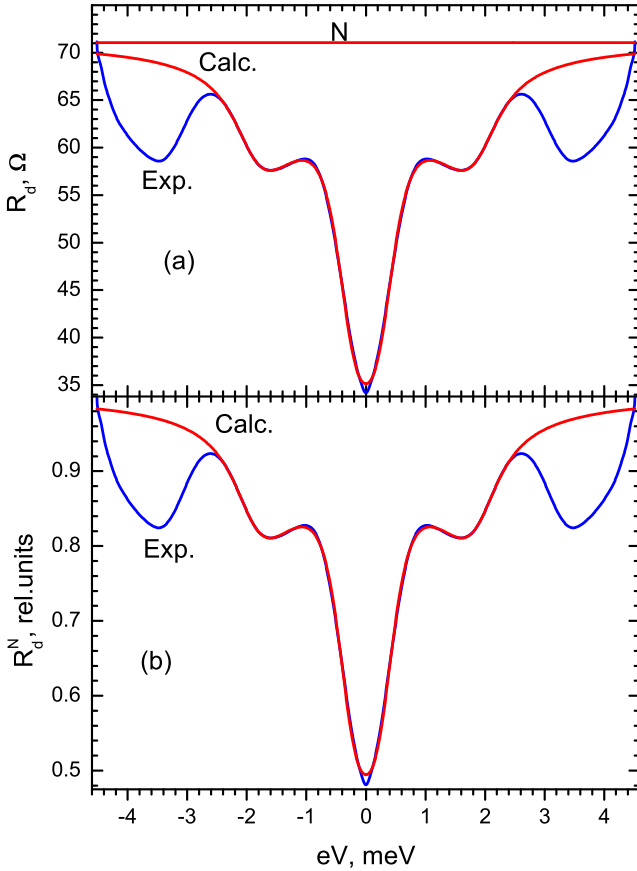


Figure 6. (a) - differential resistance of point contact  $NbSe_2 - Cu$ . Blue curve - experiment, red calculation,  $N \sim 71 \Omega$ . (b) - curves after normalization.  $\Delta_1=0.245$  meV;  $\Delta_2=1.915$  meV;  $\Gamma_1=0.0232$  meV;  $\Gamma_2=0.1$  meV;  $Z=0.346$ ; contribution from gap  $\Delta_1$ ,  $K=0.835$ ; gap contribution  $\Delta_2$ ,  $(1-K)=0.165$ , (see Eq.15);  $S_F=1.702$ ;  $2\Delta_1/kT_C=0.8$ ;  $2\Delta_2/kT_C=6.242$

to the layers is almost the same as the lattice period. The equation 15 assumes a ballistic mode of electron flight through the point contact. While this requirement can be met with respect to the impulse and energy electron path lengths within the framework of the materials and technology used to create point contacts, this is not possible with respect to the coherence lengths due to natural reasons, especially for the  $c$  direction. Nevertheless, due to the lack of an alternative, we will use the equation 15 when finding the values of the energy gaps).

The differential resistance of the  $NbSe_2 - Cu$  point contact in the superconducting state (*Exp* curve) as well as the theoretical curve (*Calc*) calculated within the framework of the modified BTK model are shown in Fig.6(a). Unfortunately, we do not have the normal-state curve. Nevertheless, we managed to find this curve for further evaluations using a simple procedure. Using parameters

of the curve *Calc*, we calculated exactly the same curve, but already normalized to the normal state with some scaling factor  $S_F$ . After that we divided the original calculated curve by the last one. By the method of successive approximations, varying  $S_F$ , we achieved that as a result of such division a horizontal segment of a straight line is obtained. Its position on the ordinate axis corresponds to the value of resistance of the point contact in the normal state. The energy gap values obtained as a result of the fitting correlate well with those obtained, for example, with tunnel contacts, see, e.g., [27]. In spite of the fact that the values of superconducting energy gap  $\Delta_1$  and  $\Delta_2$  differ practically 8 times, and one would assume an appreciable difference of Fermi electron parameters in different zones, nevertheless it was possible to obtain an excellent agreement on the form of calculated and experimental curve using the same for both gaps tunneling parameter  $Z$  in the fitting process. The deviation in shape from the calculated curve at displacements over 2.5 mV is apparently due to the presence at  $3 \div 6$  mV of a group of phonons associated with charge density waves (CDWs) [28]. Static distortions of the lattice caused by CDWs result in a superstructure with a period approximately triple that of the original lattice. The occurrence of the superlattice leads to the aforementioned low-energy CDWs phonons. In [29] it is shown that for superconductors with strong EPI (for contacts with direct conductivity, taking into account the elastic component of the current leads to additional nonlinearity associated with the dependence of the superconducting gap on the bias on the contact and caused by the electronic-phonon reformation of the energy spectrum of the superconductor. It is shown there that elastic processes lead to the appearance of differential conductivity maxima in the region of characteristic phonon energies on the first derivative of the excess current, which is observed in our experiment. Note that previously we observed a similar manifestation of elastic scattering processes in lead and indium [30] point contacts. It is important to emphasize that along with elastic scattering processes, in superconducting contacts with direct conductivity also coexist inelastic phonon scattering processes on Andreev electrons, which leads to a reduction of the excess current. That is, in this case, phonon features manifest themselves in the form of differential resistance maxima of the excess current. Thus, these contributions are directed oppositely to each other and can mutually weaken. Moreover, it is difficult to estimate in advance which contribution will

be predominant, much depends on external conditions.

As for the use of the same tunneling parameter  $Z$  for both purposes in two-gap superconductors (see Eq.(15)), we used this approach to study the gap structure in nickel borocarbide compounds [11, 14, 31, 32] and obtained an excellent agreement between the experimental and calculated characteristics of the point contacts studied.

Let's pay attention to the fact that the tunneling parameter of our point contact ( $Z=0.346$ ) is very close to the theoretical estimate for the point contact  $Ta - Cu$  with perpendicular electrons falling on the interface ( $Z=0.385$ , Fig.1). The point contact resistances are also very close to each other ( $R_N=73\Omega$  for  $Ta - Cu$  and  $R_N=71\Omega$  for  $NbSe_2$ ). As noted in the theoretical section of the article, knowing the diameter of the homocontact, you can calculate the diameter of the heterocontact, and the result of the calculation does not depend on which side of the metal was calculated. Thus, given that in both cases one of the banks is copper, we can assume that the diameters of the point contacts are very close to each other, an estimate of  $d \sim 8.5$  nm. Since the coherence length perpendicular to the layers is approximately the same as the lattice period in the same direction, and the lattice period contains 2 monolayers, it follows from this estimate that at least four  $NbSe_2$  monolayers adjacent to the hole fall into the current concentration region. To summarize, the ballistic condition with respect to the coherence length is clearly violated, while at the same time the elastic and inelastic relaxation lengths are noticeably larger than the contact size. The applicability of modified BTK theory to these kinds of contacts turned out to be quite satisfactory except for the intensity of the spectra: the scale factor  $S_F$  was 1.7 times the theoretical expectation, which manifested itself in a doubling of the differential resistance at the transition to the normal state (Fig.6(a))  $R_0 \approx 35 \Omega$ ;  $R_N \approx 70 \Omega$ .  $R_0 \approx 35 \Omega$ ;  $R_N \approx 70 \Omega$ ;

Fig.7 shows the second derivative and the  $I - V$  curve of the same contact in a wider energy range. As can be seen from the figure, at voltages above 4.5 mV the transition of the  $I - V$  curve to a new branch with a large differential resistance is observed. The transition mechanism here is similar to that in  $Ta - Cu$  point contacts. Electrons with excess energy  $eV$ , scattering on low-energy CDWs-phonons, lose energy and accumulate above the gap. In tantalum, the concentration growth of nonequilibrium quasiparticles occurs in a large volume with a size on the order of the coherence length

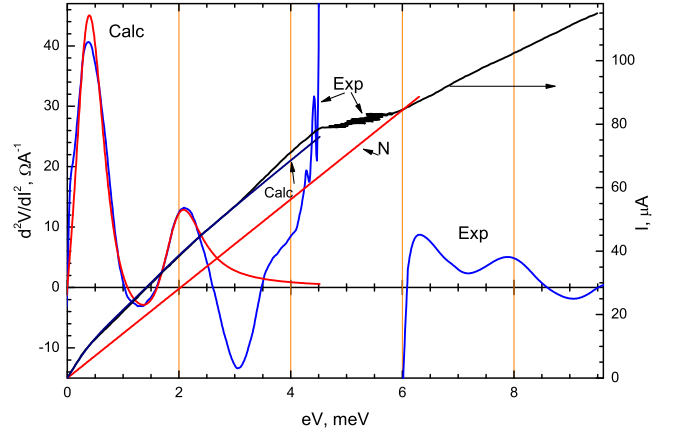


Figure 7.  $I - V$  curve and its second derivative for the  $NbSe_2 - Cu$  point contact,  $T=1.7$  K,  $H=0$ . *Exp* - experimental data, *Calc* - calculated curve, *N* - normal state approximation (see Fig.6).

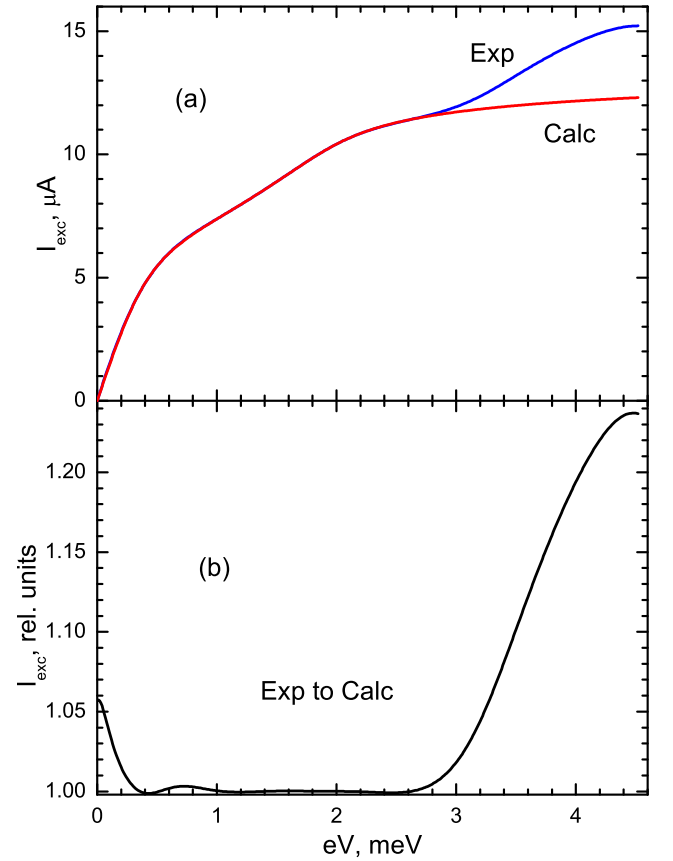


Figure 8. (a) - excess current for the curves shown in Fig.7. (b) is the relative magnitude of the excess current from the bias.

( $\xi_0 \sim 90$  nm), which promotes a smooth phase transition to the suppressed gap state. In the case of  $NbSe_2$ , however, the transition to the nonequilibrium state occurs in the layer adjacent to the contact and located in the current concentration region. In this case, the smallest fluctuations in the current strength caused by external inductions lead to fluctuations in the concentration of nonequilibrium quasiparticles, which manifests itself in the corresponding form of the  $I - V$  curve. After reaching the critical concentration and phase transition of two monolayers into the nonequilibrium state with a suppressed gap, the  $I - V$  curve moves to a branch with a large differential resistance (see also Fig.11(b),  $N \sim 71 \Omega$  – linear approximation of the normal state differential resistance,  $R_d \sim 120 \Omega$  – quasilinear approximation of the new branch), similar to what took place for the  $Ta - Cu$  contact.

In Fig.8, panel (a) shows the experimental and calculated dependences of the excess current before the transition of the superconductor into a nonequilibrium state, in panel (b) - the experimental value normalized to the calculated value. As follows from the figure, the increase of the superconducting gap due to elastic processes of electron-phonon reformation of the superconductor energy spectrum, leads to an increase in the excess current by approximately 24% compared to the calculation.

Fig.9 shows the  $I - V$  curves, first and second derivatives of the same point contact in the whole bias range. In panel (a) tangents are drawn to the sections of the  $I - V$  curves, designated by numbers 2, 3 and 4. As can be seen from the figure, on these quasi-linear sections of the  $I - V$  curve the differential resistance changes in jumps, resembling the features caused by the formation of phase slip centers in a thin superconducting filament. The differential impedance of the tangent sections of the  $I - V$  curve 2, 3, and 4 (panel (a)) is 120, 150, and 173  $\Omega$  (see panel (b)); the incremental differential impedance is 30 and 23  $\Omega$ . Note the large hysteresis loop between curves 2 and 3; the figure shows the maximum loop obtained. During multiple recordings, branch-to-branch breaks could occur under the action of the leads at other points as well. The reason for the appearance of such a stepped structure of the  $I - V$  curve is the layered structure of  $2H - NbSe_2$ . While strong covalent chemical bonds are present within each layer, neighboring layers are held together by the much weaker van der Waals interaction. As already noted, the coherence length perpendicular to the layers practically coincides with the lattice period con-

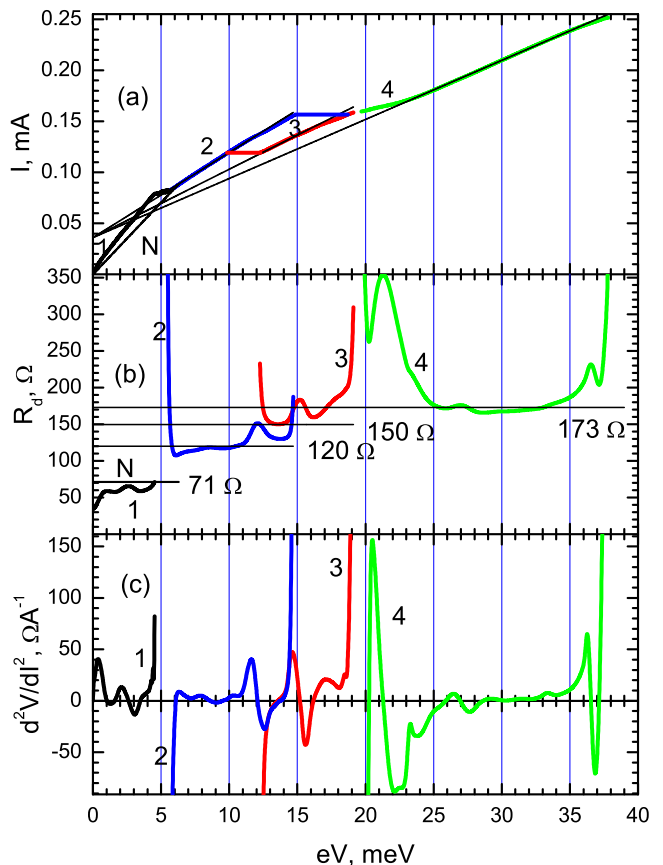


Figure 9. (a)  $I - V$  curve of the  $NbSe_2 - Cu$  point contact,  $T=1.7$  K. The step plots are marked with numbers 1-4. Tangents to them are drawn by thin lines.  $N$  is the normal state line. (b) Differential resistances for the plots of the panel  $I - V$  curve (a). Thin lines correspond to the tangents for these sections. (c) Second derivatives for the corresponding sections.

taining 2 monolayers. And since the conversion of Andreev electrons to Cooper pairs occurs at a distance of the order of the coherence length, the maximum value of the superconducting current is reached at the boundary of the lattice period. In fact, due to the weak coupling between the layers, when the value of the critical current is exceeded, the weak coupling begins to generate a flux of normal quasiparticles. Since the energy range of quasiparticles with energy  $0 < \epsilon < eV$  is significantly larger than the contact size, the inelastic relaxation in the second pair of layers united by a common coherence length causes the non-equilibrium quasiparticles to accumulate above the gap, but their concentration is still less than critical to pass to the non-equilibrium state. Therefore, the transition of the Josephson coupling between the first and second pairs of layers into a resistive



state sharply increases the flux of nonequilibrium quasiparticles into the second pair and switches it into the nonequilibrium state with the suppressed gap. The hysteresis loop arises because before the switching we had an asymmetric Josephson transition, in which in the first pair the gap was suppressed and in the second pair it had an equilibrium state. After switching the second pair, we had a symmetric Josephson transition with suppressed gap, and the reversal of the  $I - V$  curve goes on a branch with a large differential up to the second pair transition again to the state with the equilibrium gap. Note, the transition from branch to branch for the maximum hysteresis loop occurs around the maximums of differential resistance of point contacts on the first derivative of the  $I - V$  curve (panel b). These maxima correspond to the phonon state density maxima. Near these phonon peaks, there is a faster change in the concentration of nonequilibrium quasiparticles above the gap due to scattering of quasiparticles with maximum energy  $eV$  on nonequilibrium phonons. Switching from branch to branch at other points of this hysteresis loop is due to random inductions.

Thus, the sequential transition of the three pairs of layers adjacent to the contact into the nonequilibrium state with a suppressed gap is accompanied by a change in the quasilinear differential resistance from  $71 \Omega$  (normal state approximation) to, respectively, 120, 150 and  $171 \Omega$  and a decrease in the increment 49, 30 and  $23 \Omega$ . The number of pairs of  $2H - NbSe_2$  layers that have moved to the nonequilibrium state gives us an independent estimate of the contact diameter. The three pairs in the current concentration region give an estimate for the diameter  $d \sim 15$  nm. This diverges somewhat from the original estimate of the contact diameter. A possible reason for this is the slightly higher value of the tunneling parameter compared to the estimate for the tantalum-based contact, and the possible deviation of the contact shape from the hole model or the scaling factor value from 1, which gives an overestimate of the normal resistance approximation, when perhaps the estimates should have relied on the zero-displacement pulling resistance at the contact, taking into account the associated factors.

## 5. DISCUSSION

For the phase transition of a superconductor to the nonequilibrium state with a suppressed gap, it is necessary and sufficient to increase the concentration of nonequilibrium quasiparticles above the critical one

above the gap in a layer of order  $\Delta$  above the ceiling of the energy gap. To achieve the critical concentration, double tunneling contacts are often used. In such structures, one of the contacts is a low-resistance tunneling junction that creates a nonequilibrium superconducting state (generator) in the middle film. The second contact is higher impedance to introduce a minimum of perturbations into the middle film and serves to obtain information about this state (detector) [33]. Due to the geometry of the experiment, varying the flux of nonequilibrium quasiparticles with the desired energy is quite simple.

In three-dimensional point contacts whose size  $d$  is substantially smaller than the impulse  $l_i$  and energy  $l_e$  relaxation length of electrons and phonons  $l_{ph}$  there is no local equilibrium between electrons and lattice. When current passes through the  $N - S$  contact in the superconducting electrode there is no equilibrium between quasi-particle excitations and condensate, manifested in the imbalance of the occupancies of the electron- and hole-like branches of the quasi-particle excitation spectrum. One consequence of this is the reverse flux of quasiparticles, leading to an increase in the differential resistance of the point contact. With increasing current in the superconductor in the vicinity of the contact the total concentration of quasiparticle excitations also increases, which leads to the suppression of the gap, and when the critical concentration is reached, the transition to a spatially inhomogeneous nonequilibrium state occurs. Electron reabsorption of nonequilibrium phonons plays a decisive role in the accumulation of quasiparticle excitations above the gap. The multiplication of quasiparticles by reabsorption of nonequilibrium phonons leads to an increase in the total number of quasiparticles and to a decrease in the gap near the contact. The steady-state concentration of nonequilibrium quasiparticles is determined by the ratio of generation and recombination rates. The recombination rate increases with temperature, so when the temperature rises, the critical concentration is reached at higher injection powers, and the nonequilibrium feature shifts to the region of higher energies. Since the minimal volume of a superconductor in which the phase transition to the nonequilibrium state with a suppressed gap cannot be smaller than the coherence length in size, the realization of the critical concentration of quasiparticles in superconductors with large  $\xi$  at bias within phonon spectrum energies is impossible, what is easily achieved by double tunnel structures, is unattainable for three-dimensional point contacts.

Finally, a very important observation. As the experiment shows, nonequilibrium features were never observed in dirty point contacts, the perfection of the superconductor crystal lattice plays a very important role. For example, in dirty tantalum-based point contacts there were no nonequilibrium features in the spectra. A similar observation applies to niobium-based point contacts. The presence of a clear step structure of the HTSC  $I - V$  curve, associated with the discrete character of the electric field penetration into the region of the point contact contraction was also observed in samples with a high degree of crystal order in the contraction [23, 34].

## 6. CONCLUSION

1. It was found that after the transition of the superconductor region to a nonequilibrium state, this state turns out to be stable to changes in the injection power (the excess current and, consequently, the energy gap, change very insignificantly in a wide range of biases.
2. It was found that the transition of the supercon-

ductor region to the nonequilibrium state with a reduced gap is possible only for an unperturbed superconductor with a perfect lattice.

3. It is shown that the increase in the differential resistance of the point contact during the transition to a nonequilibrium state occurs due to the appearance of unbalanced occupancy of the hole and electronic branches of the quasiparticle excitation spectrum, which leads to the appearance of reverse current and the additional voltage associated with it.
4. It is found that the use of the modified BTK equations for pure superconducting point contacts with a coherence length smaller than the diameter, leads to overestimated values of the amplitude (or intensity) of the gaps.
5. The possibility of estimating the value of the normal resistance of a point contact using its superconducting characteristics is shown.

The work was supported by the National Academy of Sciences of Ukraine within the F19-5 project.

- 
1. I.K. Yanson, L.F. Rybal'chenko, N.L. Bobrov, and V.V. Fisun, *Fiz. Nizk. Temp.* **12**, 552 (1986) [*Sov. J. Low Temp. Phys.* **12**, 313 (1986)], [arXiv.1512.00684](#)
  2. I.K. Yanson, N.L. Bobrov, L.F. Rybal'chenko, V.V. Fisun, *Fiz. Nizk. Temp.* **13**, 1123 (1987) [*Sov. J. Low Temp. Phys.* **13**, 635 (1987)] [arXiv.1512.03917](#)
  3. R.C. Dynes, V. Narayanamurti, and J.P. Garno *Phys. Rev. Lett.* **39**, N4, 229 (1977)
  4. N.L. Bobrov, L.F. Rybal'chenko, V.V. Fisun, I.K. Yanson, *Fiz. Nizk. Temp.*, **13**, 611 (1987); *Sov. J. Low Temp. Phys.*, **12**, 344 (1987); [arXiv.1512.01800](#)
  5. R.I. Shekhter and I.O. Kulik, *Fiz. Nizk. Temp.* **9**, 46 (1983) [*Sov. J. Low Temp. Phys.* **9**, 22 (1983)].
  6. G. Bambakidis, *Phys. Status Solidi (b)* **54**, K57 (1972).
  7. M.H. Halloran, J.H. Condon, J.E. Graebner, J.E. Kunzler, F.S.L. Hsu, *Phys. Rev. B* **1**, 366, (1970).
  8. V.V. Ryazanov, V.V. Schmidt and L.A. Ermolaeva, *J. Low Temp. Phys.* **45**, No. 5/6, 507 (1981).
  9. M.J.G. Lee, J. Caro, O.G. Croot, R. Griessen. *Phys. Rev. B* **31**, No. 12, 8244 (1985).
  10. G.E. Blonder, M. Tinkham, and T.M. Klapwijk, *Phys. Rev. B* **25**, 4515 (1982).
  11. N.L. Bobrov, S.I. Beloborod'ko, L.V. Tyutrina, I.K. Yanson, D.G. Naugle, and K.D.D. Rathnayaka, *Phys. Rev. B* **71**, 014512 (2005).
  12. A.V. Zaitsev, *Sov. Phys. JETP* **59**, 1015 (1984) [*Zh. Eksp. Teor. Fiz.* **86**, 1742 (1984)]
  13. Yu.G. Naidyuk, K. Gloos, *Low Temperature Physics* **44**, 257–268 (2018) [*Fiz. Nyzk. Temp.*, **44**, 343–356 (2018).]
  14. N.L. Bobrov, V.N. Chernobay, Yu.G. Naidyuk, L.V. Tyutrina, I.K. Yanson, D.G. Naugle, K.D.D. Rathnayaka, *Fiz. Niz. Temp.*, **36**, N10-11, p.1228-1243, (2010) [*Low Temperature Physics* **36**, 990-1003 (2010)]; [arXiv:1006.5933 \[cond-mat.supr-con\]](#)
  15. V.E. Startsev, "Local singularities in the Fermi surfaces and electronic transport phenomena in transition metals" Author's Abstract of Doctoral Dissertation in Physical-Mathematical Sciences, Sverdlovsk (1983)
  16. N.L. Bobrov, L.F. Rybal'chenko, A.V. Khotkevich, and I.K. Yanson, *USSR Patent No. 1631626*, *Byull. Izobret.*, No. 8 (1991).
  17. P.N. Chubov, A.I. Akimenko, and I.K. Yanson, *USSR Patent No. 834803*, *Byull. Izobret.*, No. 20 (1981), p. 232.
  18. I.I. Mazin, A.A. Golubov, and B. Nadgorny, *J. Appl. Phys.* **89**, 7576 (2001).
  19. N.L. Bobrov, *J. Exp. Theor. Phys.* **133**, 59–70, (2021). [arXiv.2109.01344](#)

20. A.P. van Gelder, *Solid State Comm.*, **25**, No 12, 1097 (1978)
21. N.L. Bobrov, *Low Temperature Physics* **45**, 482 (2019); [arXiv.1906.04380](#)
22. G.E. Blonder and M. Tinkham, *Phys. Rev. B* **27**, 112 (1983).
23. S.B. Kaplan, C.C. Chi, D.N. Langenberg, et al., *Phys. Rev. B* **14**, 4854 (1976).
24. I.K. Yanson, L.F. Rybal'chenko, V.V. Fisun, N.L. Bobrov, M.A. Obolenskii, M.B. Kosmyna, V.P. Seminozhenko, *Sov. J. Low Temp. Phys.*, **14**, 639 (1988) *Fiz. Nizk. Temp.*, **14**, 1157 (1988); [arXiv.1512.06416](#)
25. I.A. Gospodarev, V.V. Eremenko, K.V. Kravchenko, V.A. Sirenko, E.S. Syrkin, and S.B. Feodos'ev, *Low Temp. Phys.* **36**, 344 (2010)
26. J. Edwards, R.F. Frindt, *J. Phys. Chem. Solids* **32** 2217 (1971)
27. T. Dvir, F. Masee, L. Attias, M. Khodas, M. Aprili, C.H.L. Quay, H. Steinberg, *Nat Commun* **9**, 598 (2018).
28. N.L. Bobrov, L.F. Rybal'chenko, M.A. Obolenskii, and V.V. Fisun, *Fiz. Nizk. Temp.*, **11**, 897 (1985); (*Sov. J. Low Temp. Phys.*, **11**, 510 (1985)) DOI: [arXiv.1603.02598](#)
29. Omel'yanchuk A.N., Beloborod'ko S.I., *Sov. J. Low Temp. Phys.* **14** 630 (1988); *Fiz. Niz. Temp.* **14** 1142 (1988)
30. N.L. Bobrov, A.V. Khotkevich, G.V. Kamarchuk, P.N. Chubov, *Low Temp. Phys.* **40**, 215 (2014); *Fiz. Niz. Temp.* **40**, 280, (2014) [arXiv.1405.6869](#)
31. N.L. Bobrov, S.I. Beloborod'ko, L.V. Tyutrina, V.N. Chernobay, I.K. Yanson, D.G. Naugle, K.D.D. Rathnayaka, *Low Temperature Physics* **32**, 489 (2006); [arXiv.cond-mat/0511373](#)
32. N.L. Bobrov, V.N. Chernobay, Yu.G. Naidyuk, L.V. Tyutrina, D.G. Naugle, K.D.D. Rathnayaka, S.L. Bud'ko, P.C. Canfield, I.K. Yanson, *EPL* **83** 37003 (2008) [arXiv.0806.1456](#)
33. E.M. Rudenko *Low Temp. Phys.* **38**, 353 (2012)
34. L.F. Rybal'chenko, V.V. Fisun, N.L. Bobrov, M.B. Kosmyna, A.I. Moshkov, V.P. Seminozhenko, I.K. Yanson, *Sov. J. Low Temp. Phys.*, **15**, 54 (1989); *Fiz. Nizk. Temp.*, **15**, 95 (1989); [arXiv.1701.09124](#)